Tellus (2008), 60B, 238–249
Printed in Singapore. All rights reserved

TELLUS

A Kalman-filter bias correction method applied to deterministic, ensemble averaged and probabilistic forecasts of surface ozone

By LUCA DELLE MONACHE[1,2]*, JAMES WILCZAK[3], STUART MCKEEN[4,5], GEORG GRELL[4,6], MARIUSZ PAGOWSKI[6,7], STEVEN PECKHAM[4,6], ROLAND STULL[1], JOHN MCHENRY[8] and JEFFREY MCQUEEN[9], [1]*Atmospheric Science Programme, Earth and Ocean Sciences Department, University of British Columbia, Vancouver, British Columbia, Canada;* [2]*Now at Lawrence Livermore National Laboratory, Livermore, CA, USA;* [3]*Physical Sciences Division, Earth System Research Laboratory, National Oceanic and Atmospheric Administration, Boulder, CO, USA;* [4]*Cooperative Institute for Research in Environmental Sciences, University of Colorado, Boulder, CO, USA;* [5]*Chemical Sciences Division, Earth System Research Laboratory, National Oceanic and Atmospheric Administration, Boulder, CO, USA;* [6]*Global Systems Division, Earth System Research Laboratory, National Oceanic and Atmospheric Administration, Boulder, CO, USA;* [7]*Cooperative Institute for Research in the Atmosphere, Colorado State University, Fort Collins, CO, USA;* [8]*Baron Advanced Meteorological Systems, c/o North Carolina State University, Raleigh, NC, USA;* [9]*National Weather Service / National Centers for Environmental Prediction/National Oceanic and Atmospheric Administration, Camp Springs, MD, USA*

(Manuscript received 26 June 2007; in final form 12 November 2007)

ABSTRACT

Kalman filtering (KF) is used to estimate systematic errors in surface ozone forecasts. The KF updates its estimate of future ozone-concentration bias using past forecasts and observations. The optimum filter parameter is estimated via sensitivity analysis. KF performance is tested for deterministic, ensemble-averaged and probabilistic forecasts. Eight simulations were run for 56 d during summer 2004 over northeastern USA and southern Canada, with 358 ozone surface stations.

KF improves forecasts of ozone-concentration magnitude (measured by root mean square error) and the ability to predict rare events (measured by the critical success index), for deterministic and ensemble-averaged forecasts. It improves the 24-h maximum ozone-concentration prediction (measured by the unpaired peak prediction accuracy), and improves the linear dependency and timing of forecasted and observed ozone concentration peaks (measured by a lead/lag correlation). KF also improves the predictive skill of probabilistic forecasts of concentration greater than thresholds of 10–50 ppbv, but degrades it for thresholds of 70–90 ppbv. KF reduces probabilistic forecast bias. The combination of KF and ensemble averaging presents a significant improvement for real-time ozone forecasting because KF reduces systematic errors while ensemble-averaging reduces random errors. When combined, they produce the best overall ozone forecast.

1. Introduction

The skill of deterministic ozone forecasts can be improved using ensemble methods (e.g. Delle Monache and Stull, 2003; McKeen et al., 2005; Delle Monache et al., 2006a, Mallet and Sportisse, 2006; Wilczak et al., 2006; Thunis et al., 2007; van Loon et al., 2007), by combining weighted ensemble averaging with the application of linear regression (Pagowski et al., 2005) or dynamic linear regression (Pagowski et al., 2006), and with bias removal methods (e.g. McKeen et al., 2005; Wilczak et al., 2006; Delle Monache et al., 2006b, hereinafter referred to as DM06b).

Forecast bias (i.e. systematic error) is a problem common to all chemistry transport models (CTMs) (Russell and Dennis, 2000). This study evaluates the ability of the Kalman filter (KF) predictor post-processing bias-removal method in predicting biases of surface ozone forecasts. The KF correction is an automatic post-processing method that uses past observations and forecasts

*Corresponding author.
e-mail: ldm@llnl.gov

DOI: 10.1111/j.1600-0889.2007.00332.x

Table 1. General information about the eight photochemical models used in this study

Model, organization	Driving meteorology	Chemical mechanism	Horizontal spatial resolution (km)
AURAMS, Meteorological Service of Canada	GEM (Côtè et al., 1998a,b)	ADOM II (Lurman, 1986; Atkinson et al., 1992)	42
CHRONOS, Meteorological Service of Canada	GEM (Côtè et al., 1998a,b)	ADOM II (Lurman, 1986; Atkinson et al., 1992)	21
BAMS-15, Baron Advanced Meteorological System Inc. Corporation	MM5 (Grell et al., 1994)	CB-IV (Gery et al., 1989)	15
BAMS-45, Baron Advanced Meteorological System Inc. Corporation	MM5 (Grell et al., 1994)	CB-IV (Gery et al., 1989)	45
CMAQ/ETA, National Weather Service/ National Center for Environmental Prediction	NWS/NCEP ETA (McQuenn et al., 2004)	CB-IV (Binkowski and Shankar, 1995)	12
WRF/CHEM-1, NOAA Global Systems Division	WRF (Grell et al., 2005)	RADM2 (Stockwell et al., 1995)	27
WRF/CHEM-2, NOAA Global Systems Division	WRF (Grell et al., 2005)	RADM2 (Stockwell et al., 1995)	27
STEM, University of Iowa	MM5 (Grell et al., 1994)	SAPRC-99 (Carter, 2000)	12

to estimate the model bias in the future forecast. Here bias is defined as the 'the mean systematic error' (Jolliffe and Stephenson, 2003).

The data set used in this study to test the KF was collected during the International Consortium for Atmospheric Research on Transport and Transformation/New England Air Quality Study (ICARTT/NEAQS). The experiment, including both ozone surface and upper air observations and predictions [archived by the National Oceanic and Atmospheric Administration (NOAA) Earth System Research Laboratory], was held during summer of 2004 over northeastern USA and southern Canada. The following eight CTM simulations from seven models (as described also in Table 1) were run from 0000 UTC 6 July to 0000 UTC 30 August 2004 (i.e. 56 d):

(1) A unified Regional Air-quality Modeling System (AURAMS) (Moran et al., 1997) and the Canadian Hemispheric and Regional Ozone and NO_x System (CHRONOS) (Pudykiewicz et al., 1997) provided by the Meteorological Service of Canada.

(2) The Baron Advanced Meteorological System Multi-scale Air Quality Simulation Platform (McHenry et al., 2004), run at 15 km (BAMS-15) and 45 km (BAMS-45), provided by Baron Advanced Meteorological System Inc. Corporation.

(3) The Community Multi-scale Air Quality Model (CMAQ/ETA) (Byun and Schere, 2006) from the National Weather Service (NWS)/National Center for Environmental Prediction (NCEP).

(4) The Weather Research and Forecast Model/Chemistry model (Grell et al., 2005) run with two different versions [version 1.3 (WRF/CHEM-1) and version 2.03 (WRF/CHEM-2)] by the NOAA Global Systems Division. WRF/CHEM is an on-line CTM, where the chemistry is fully coupled with the meteorology.

(5) The Sulfur Transport and Emissions Model (STEM) (Carmichael et al., 2003) provided by University of Iowa.

Hourly averaged surface ozone measurements were available at roughly 360 stations and stored in the Aerometric Information Retrieval Now (AIRNow) database. Since the KF is applied directly to hourly data, the filter correction effect is studied here by analysing hourly ozone concentration data. As found in other studies (McKeen et al., 2005; Wilczak et al., 2006) efficient bias removal procedures applied to 1-h ozone predictions also improve 8-h concentration predictions, which is the Environmental Protection Agency (EPA) time resolution for ozone exceedences and exposure standards. The model domains, their overlap, and the station characterizations are shown in Fig. 1. Further

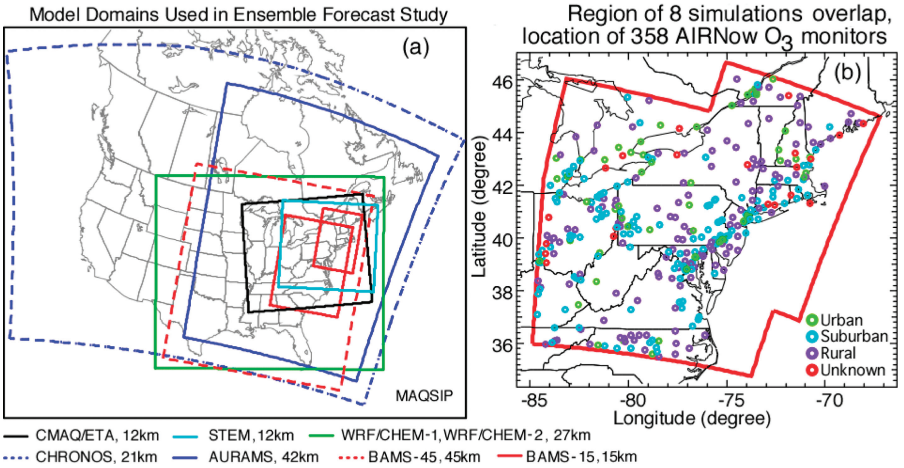

Fig. 1. (a) The eight photochemical simulation domains. CMAQ/ETA (solid black line), STEM (solid cyan line), WRF/CHEM (solid green line), CHRONOS (dotted blue line), AURAMS, (solid blue line), BAMS-45 (dotted red line) and BAMS-15 (solid red line). (b) Domains overlap (solid red), including stations subdivided by urban (green circles), suburban (cyan circles), rural (purple circles) and unknown classification (red circles).

details about each model and the observation data can be found in McKeen et al. (2005).

DM06b showed that the KF-corrected deterministic and ensemble-averaged forecasts are improved for correlation, gross error, root mean square error (RMSE), and unpaired peak prediction accuracy (UPPA). They applied Kalman filtering to a 5-d ozone episode for five surface ozone stations in western Canada during summer of 2004. Their preliminary successful results prompted this extended analysis, for a 56-d case study during summer of 2004 with 360 surface ozone stations over northeastern USA and southern Canada. Moreover, the KF predictor bias-removal method is applied here for the first time to evaluate probabilistic surface ozone forecasts. The extended ICARTT/NEAQS data set also allowed a sensitivity analysis for a key filter parameter, for which an optimal value is found.

The KF method and algorithm are described in Section 2, along with a sensitivity analysis of the error-ratio filter parameter. An optimal value for this parameter is found by evaluating the KF performance with different meteorology and air quality (AQ) scenarios. Using this optimal value of the error-ratio the filter performance is tested for deterministic, ensemble-averaged (Section 3) and probabilistic surface ozone forecasts (Section 4). In Section 5 conclusions are drawn from those results.

2. The Kalman filter and its optimum parameter

The KF has been used in data-assimilation schemes to improve the accuracy of the initial conditions for numerical weather prediction (e.g. Hamill and Snyder, 2000) and AQ forecasts (e.g. van Loon et al., 2000). The KF has also been used for weather and AQ (i.e. ozone) forecasts as a predictor bias-correction method during post-processing of short-term forecasts (Homleid, 1995; DM06b). The latter approach is applied here. The filter uses a recursive algorithm to estimate the systematic component of the forecast error, effectively reducing the bias that often corrupts AQ forecasts (e.g. Russell and Dennis, 2000; DM06b).

The KF predictor–corrector approach is linear, adaptive, recursive and optimal. Namely, it predicts the future bias with a linear relationship, given by the previous bias estimate plus a quantity proportional to the difference between the present forecast error and the previous bias estimate. The KF approach adapts its coefficients during each iteration, resulting in a short training period. However, KF is unable to predict a large bias when all biases for the past few days have been small. KF is recursive because at any iteration values of the KF coefficients depend on the values at the previous iteration. Finally, KF is optimal in a least-square-error sense (DM06b).

2.1. Filter algorithm

A detailed description of the filter algorithm can be found in DM06b. Here only the definitions of the error variances are shown, because the ratio of these variances is an important parameter that affects the KF performance. Sensitivity tests of this ratio are presented in the next subsection.

The true (unknown) forecast bias x_t is modelled at time t by the previous true bias plus a white noise η term (Bozic, 1994):

$$x_{t|t-\Delta t} = x_{t-\Delta t|t-2\Delta t} + \eta_{t-\Delta t}. \tag{1}$$

Here $\eta_{t-\Delta t}$ is assumed to be uncorrelated in time and normally distributed with zero-mean and variance σ_η^2, $t|t - \Delta t$ denotes dependence of the variable at time t on values at time $t - \Delta t$. The forecast error y_t (forecast minus observation at time t) is assumed to have been corrupted from true forecast bias by a random error term ε_t:

$$y_t = x_t + \varepsilon_t = x_{t-\Delta t} + \eta_{t-\Delta t} + \varepsilon_t, \tag{2}$$

where again ε_t is assumed uncorrelated in time and normally distributed with zero-mean and variance σ^2_ε. Thus, y_t includes systematic and random errors.

2.2. *Error-ratio parameter sensitivity tests*

The KF performance is sensitive to the error ratio $\sigma^2_\eta/\sigma^2_\varepsilon$. If the ratio is too high, the forecast-error white-noise variance (σ^2_ε) will be relatively small compared to the true forecast-bias white-noise variance (σ^2_η). Therefore, the filter will put excessive confidence on the previous forecast, and the predicted bias will respond very quickly to previous forecast errors. On the other hand, if the ratio is too low, the predicted bias will change too slowly over time. Consequently, there exists an optimal value for the ratio that is given by the climatology of the forecast region, which can be estimated by evaluating the filter performance in different situations with different meteorology and different AQ scenarios (not only for a single AQ episode as in DM06b). In this study, an optimal value is found that improves real-time surface ozone forecasts for the largest number of ozone cases, with the largest number of simulations. Nevertheless, it is recognized that predictions over different areas (e.g. rural versus urban), or different model forecasts may have different optimal ratio values.

As described in Section 1, the ICARTT/NEAQS data set offers a unique opportunity to thoroughly test the filter performance, both because of its duration (56 d of summer 2004), and due to the inclusion of eight different photochemical simulations. The raw and KF-corrected predictions from these simulations can be tested against surface observations from roughly 360 stations (for hourly ozone concentrations over the Northeast United States and Southeast Canada; McKeen et al., 2005). Specifically, with the ICARTT/NEAQS data set, an optimal error-ratio value can be estimated to produce a more accurate correction of ozone forecasts with the KF post-processing predictor method.

DM06b used a ratio value (0.01) from previous studies where the KF was used to bias-correct weather forecasts, close to the optimal value (0.06) found by Homleid (1995), who tested the filter for weather forecasts as well. Here the optimal ratio value (for ozone surface forecasts) is found by looking at the average value of the following statistical parameters over the available surface ozone stations:

1. Pearson product-moment coefficient of linear correlation (herein 'correlation'):

$$\text{correlation} = \frac{\sum_{i=1}^{N_\text{point}} \left\{[C_o(i) - \overline{C_o}][C_p(i) - \overline{C_p}]\right\}}{\sqrt{\sum_{i=1}^{N_\text{point}} \left[C_o(i) - \overline{C_o}\right]^2 \sum_{i=1}^{N_\text{point}} \left[C_p(i) - \overline{C_p}\right]^2}} \qquad (3)$$

2. RMSE:

$$\text{RMSE} = \sqrt{\frac{1}{N_\text{point}} \sum_{i=1}^{N_\text{point}} [C_p(i) - C_o(i)]^2}. \qquad (4)$$

Here N_point is the number of all valid observation/prediction couples of 1-h average concentrations over the 56-d period and 358 stations, $C_o(i)$ is the 1-h average observed concentration at a monitoring station for hour t, $C_p(i)$ is the 1-h average predicted concentration at a monitoring station for hour t, $\overline{C_o}$ is the average of 1-h average observed concentrations over all the N_point observation/prediction couples available, and $\overline{C_p}$ is the average of 1-h average predicted concentrations over all the N_point observation/prediction couples available.

Correlation determines the extent to which the observed and predicted ozone concentration values are linearly related. RMSE gives important information about the skill of a forecast in predicting the magnitude of ozone concentration. It is also very helpful for understanding the filter performance, because it can be decomposed into systematic and unsystematic components (Section 3.2).

Since KF is optimal in a least-square-error sense (i.e. is designed to reduce RMSE) the filter optimum is chosen by evaluating its sensitivity with the RMSE metric. Correlation is included in this sensitivity analysis to assure the validity of the chosen optimal value determined from RMSE. Figures 2 and 3 show the correlation and RMSE values, respectively, for the eight models, with the ratio assuming values from 0.01 to 10 in increments of 0.01 (shown on a logarithmic scale). Both statistical parameters show KF sensitivity to the ratio values, with more pronounced differences for RMSE (Fig. 3). Correlation values have their

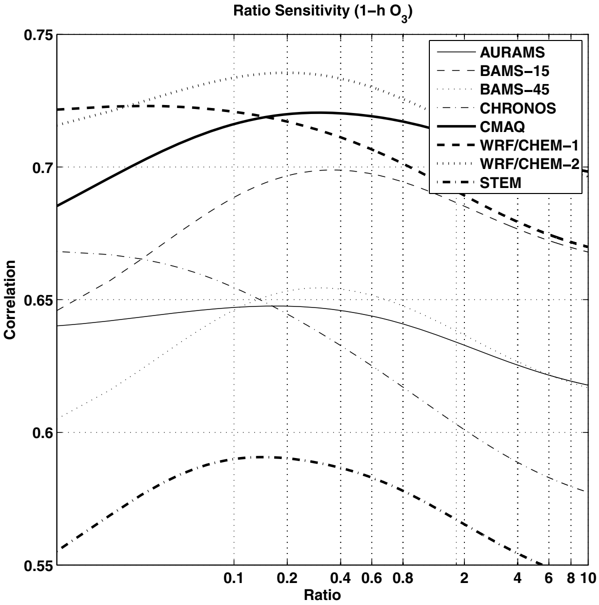

Fig. 2. Correlation values (Equation 3) for the eight photochemical simulations: AURAMS (light solid line), BAMS-15 (light dashed line), BAMS-45 (light dotted line) CHRONOS (light dash–dotted line), CMAQ/ETA (solid line), WRF/CHEM-1 (dashed line), WRF-CHEM-2 (dotted line), STEM (dash–dotted line). Values are computed with sigma error-ratio ranging from 0.01 to 10, in increments of 0.01 (shown on a logarithmic scale). Values are within the interval [−1, 1], with correlation = 1 being the best possible value.

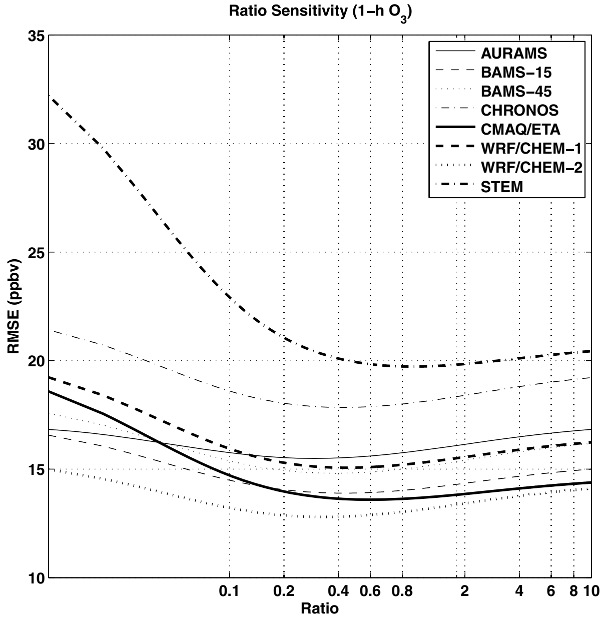

Fig. 3. As Fig. 2, but for root mean square error (RMSE) (ppbv) (eq. 4). Values within the interval [0, +∞), with a perfect forecast when RMSE = 0.

maxima and RMSE their minima roughly between 0.2 and 0.4 and in the neighbourhood of 0.4, respectively.

Based on the above sensitivity analysis, an optimal ratio value of 0.4 will be used for the remainder of this study. This value appears to be robust in that it is nearly the same for each of the models tested during the ICARTT/NEAQS study. This value is considerably higher than values used in other studies (e.g. 0.01 in DM06b and Roeger et al., 2003; and 0.06 in Homleid, 1995). One possible explanation for this difference may be the fact that previous studies found optimal ratio values by applying KF to meteorological variables (temperature, wind speed and direction, and precipitation as in Roeger et al., 2003 and temperature as in Homleid, 1995) whose biases over a diurnal cycle may have different characteristics than those of surface ozone concentration. Also, because the summer of 2004 was unseasonably cool with very few pollution episodes due to the frequent presence of continental polar air masses during July and the influence of several hurricanes, the optimum KF-variance ratio found here might not apply to other air-quality situations in other locations.

3. Deterministic and ensemble-averaged forecasts

In this section the filter performance is tested by evaluating the skill of 10 ozone forecasts and their KF corrected versions. These forecasts include the eight individual model forecasts, the ensemble-mean (i.e. an arithmetic mean) of the raw forecasts (E), and the ensemble mean of the KF forecasts (EK). Note that for the KF corrected version of EK, KF is applied twice (in combination with ensemble averaging) to the same signal, which was found in other studies (DM06b) to have the best performance overall.

The statistical metrics used for verification are correlation and RMSE as already defined in Section 2.2 with eqs (3) and (4), respectively. Hereinafter, the correlation and RMSE values are computed by considering together all the observation/prediction pairs available from all the ozone surface stations. Similarly, the following statistical metrics have been considered:

1. UPPA:

$$\mathrm{UPPA} = \frac{1}{N_{\mathrm{day}} \times N_{\mathrm{station}}} \times \sum_{\mathrm{station}=1}^{N_{\mathrm{station}}} \left[\sum_{\mathrm{day}=1}^{N_{\mathrm{day}}} \frac{\left|C_p(\mathrm{day, station})_{\max} - C_o(\mathrm{day, station})_{\max}\right|}{C_o(\mathrm{day, station})_{\max}} \right]. \tag{5}$$

2. Critical success index (CSI):

$$\frac{B}{A + B + C}. \tag{6}$$

Here N_{day} is the number of days, N_{station} is the number of stations, $C_o(\mathrm{day, station})_{\max}$ is the maximum 1-h average observed concentration at a monitoring station over 1 d, and $C_p(\mathrm{day, station})_{\max}$ is the maximum 1-h average predicted concentration at a monitoring station over 1 d. CSI is computed for a given concentration threshold: A is the number of times the observation is below the threshold and the prediction is above it; B is the number of times both the observation and the prediction are above the threshold; and C is the number of times the observation is above the threshold and the prediction is below it.

UPPA is included in the U.S. EPA guidelines [U.S. Environmental Protection Agency, 1991] to analyse historical ozone episodes using photochemical grid models. The U.S. EPA acceptable-performance value is ±20%. UPPA is computed here as an average (over the days and stations available) of the absolute value of the normalized difference between the predicted and observed daily maximum at each station (eq. 5). This ensures that under and over prediction are weighted equally and cancellation effects are not allowed. Thus, UPPA is non-negative and only the +20% acceptance performance upper limit is used in the next sections. UPPA measures the ability of the forecasts to predict the daily ozone peak, the most harmful to our respiratory system.

CSI has been chosen as a performance measure for forecasts of rare events because model and observed exceedances are equally weighted. It is computed here for thresholds between 60 and 90 ppbv, with increments of 2.5 ppbv.

3.1. Correlation

The closer correlation is to unity, the better. Figure 4 shows the results with this parameter for the eight model forecasts, E (their ensemble-averaged), and EK (the ensemble average

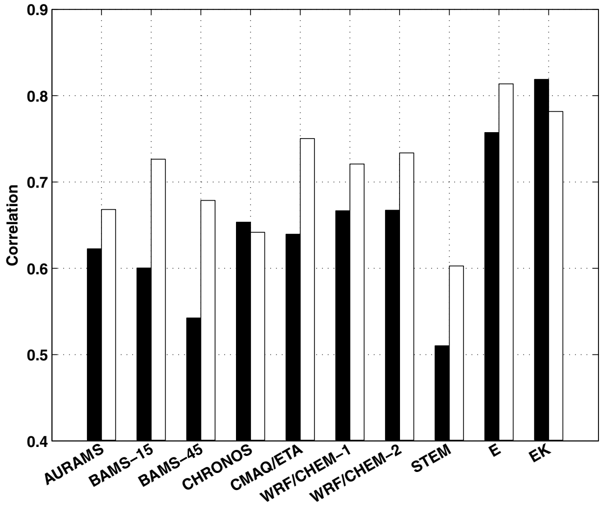

Fig. 4. Correlation values (eq. 3) for the eight models, the ensemble mean of the raw forecasts (E), and the ensemble mean of the Kalman filtered forecasts (EK). Black bars represent the raw forecasts, and white bars indicate the values for the Kalman filtered forecasts. Values are within the interval [−1, 1], with correlation = 1 being the best possible value.

of the filtered model forecasts). For each of these ten forecasts, the black bar indicates the correlation of the raw forecast with the observations, while the white bar represents correlation for the Kalman filtered forecasts. The lower and upper bounds of the computed correlation values for the 95% confidence interval differ from the values shown in Fig. 4 only in the first decimal digit. Indeed, applying a sampling uncertainty of $1/\sqrt{N}$, with $N = 421\,082$ as in this study, yields a value <1%, confirming the robustness of the computed correlation values.

Among the raw deterministic forecasts WRF/CHEM-2 has the highest correlation. Kalman filtering provides significant improvements for almost all the forecasts, ranging from 7% (AURAMS) to 24% (BAMS-45) for higher correlation values. Only the CHRONOS filtered forecast has a correlation with observations lower than its raw counterpart.

The application of the filter twice (filtered EK) did not result in any improvement (contrary to DM06b, as discussed further in the next sections), while ensemble averaging improves the correlation (higher values) for both raw and filtered forecasts. The results for E and EK suggest that applying ensemble averaging and then Kalman filtering (E, white bar, Fig. 4), or vice versa (EK, black bar, Fig. 4), is practically equivalent and provides the best forecast with this metric.

The accuracy of the forecast in predicting the timing of concentration peak and minimum values has been measured by a lead/lag correlation analysis, with correlation values between observations and predictions computed with a lag in time going from −24 to 24 h, in increments of an hour. As shown in Table 2, for the KF corrected forecasts the lag at which the maximum correlation is obtained is always lower (by 1 h, except for the WRF simulations where it is zero in both cases) than the lag of the maximum correlation between raw forecasts and observations. This means that Kalman filtering the ozone forecasts improves the accuracy of the forecast in predicting the timing of concentration peak and minimum values.

Table 2. Lag (hour) at which the correlation between observation and prediction reach its maximum

Model	Raw forecast	KF-corrected forecast
AURAMS	1	0
CHRONOS	1	0
BAMS-15	2	1
BAMS-45	2	1
CMAQ/ETA	1	0
WRF/CHEM-1	0	0
WRF/CHEM-2	0	0
STEM	1	0

3.2. *RMSE*

Following Wilmott (1981) we decompose RMSE into systematic (RMSE_s) and unsystematic (RMSE_u) (i.e. random) components to better understand the KF correction effects on the forecast skill (see DM06b for a detail description of Willmott's decomposition). RMSE_s indicates the portion of error that depends on model systematic errors (e.g. inaccurate model parameters), while RMSE_u depends on random errors and on errors resulting by a model skill deficiency in predicting a specific situation (e.g. a process not described in the model formulation). The following relationship holds between RMSE and its components:

$$\mathrm{RMSE}^2 = \mathrm{RMSE}_s^2 + \mathrm{RMSE}_u^2. \tag{7}$$

Figure 5 is built using the forecasts RMSE, RMSE_s and RMSE_u. Each arrow tail has as abscissa the raw forecast RMSE_s and as ordinate the raw forecast RMSE_u. This point distance from the origin is equal to the raw forecast RMSE. Similarly, the arrow head depicts RMSE and its components for the KF forecasts. RMSE values for both the raw and KF forecasts are reported in Fig. 5 lower right-hand corner. If an arrow is pointing to the left-hand side it means KF is reducing the forecast RMSE_s, and if it is pointing downward is reducing RMSE_u.

The closer the values of these metrics are to zero the better. RMSE is improved (lower values) for all the deterministic forecasts. E is also improved after the correction, while EK filtered version has a higher RMSE. Among the raw forecasts WRF/CHEM-2 has the lowest RMSE, while the best overall is again the unfiltered EK. Also with this metric double filtering did not provide any improvement as reported in DM06b. Ensemble averaging and Kalman filtering when combined together, regardless of the order on which these operators are applied, provide the best forecast overall (lowest RMSE).

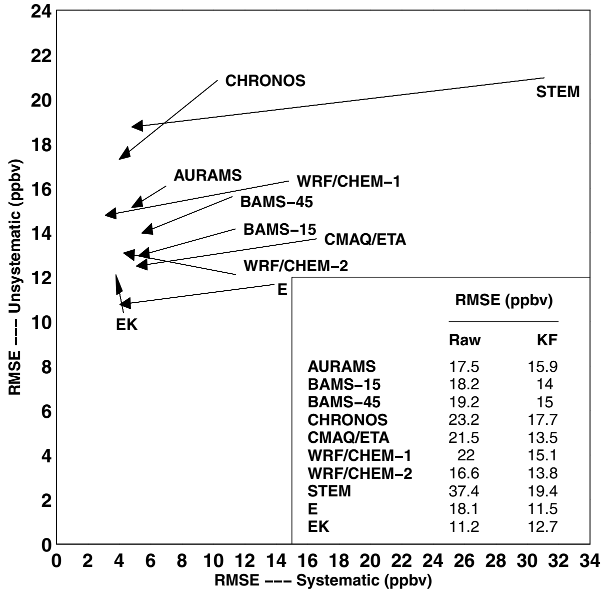

	RMSE (ppbv)	
	Raw	KF
AURAMS	17.5	15.9
BAMS-15	18.2	14
BAMS-45	19.2	15
CHRONOS	23.2	17.7
CMAQ/ETA	21.5	13.5
WRF/CHEM-1	22	15.1
WRF/CHEM-2	16.6	13.8
STEM	37.4	19.4
E	18.1	11.5
EK	11.2	12.7

Fig. 5. Root mean square error (RMSE) (eq. 4) and its systematic (RMSE_s) and unsystematic (RMSE_u) components (ppbv). Arrow tails have as abscissa the raw forecasts RMSE_s and as ordinate the raw forecasts RMSE_u. The distance between the arrow tail and the origin is equal the raw forecast RMSE. Similarly, the arrow head depicts RMSE and its components for the KF forecasts. RMSE values for both the raw and KF forecasts are reported in the lower left-hand side corner. Values are within the interval [0, $+\infty$), with a perfect forecast when RMSE = 0.

The KF is expected to correct some of the systematic components of the errors (i.e. the bias), while the random component on average (over the different forecasts) should be affected little by the filter correction (DM06b). In fact, if random errors are associated with model inadequacies, then those cannot be removed except by fundamental model improvements.

RMSE_s is improved for all the 10 forecasts after the KF correction (all arrows pointing to the left-hand side in Fig. 5), with RMSE_s improvements by 1% (for EK) up to 82% (for STEM). Ensemble averaging does not reduce systematic error. The same kind of improvements for RMSE_s have been found in DM06b, even if less pronounced than what was found in this study. The much greater duration of the data set used here and an optimal error-ratio value (as discussed in Section 2.2) allow the filter to better capture the ozone-forecast systematic errors.

Unsystematic RMSE(RMSE_u) is never substantially improved with KF, and in few cases is even higher (for WRF/CHEM-2 and EK, upward pointing arrows in Fig. 5) after the filter correction. However, ensemble averaging does reduce unsystematic error (filters out unpredictable components), confirming what was found in DM06b.

3.3. UPPA

UPPA values closer to zero are better. BAMS-15 has the lowest UPPA among the raw forecasts (Fig. 6), similar to what was found by Wilczak et al. (2006) with a running-mean bias-correction applied to the ICARTT/NEAQS data set for ozone daily peak concentrations. UPPA values are lower after the KF correction for all the deterministic forecasts, with improvements more pronounced than those presented in DM06b. This confirms the benefits of providing the filter with a much longer period to better learn the bias behaviour, as well as the benefit of an optimal sigma error-ratio value.

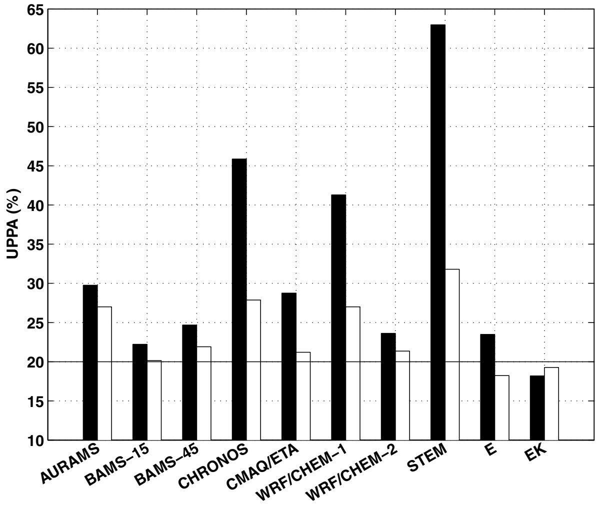

Fig. 6. As Fig. 4, but for the unpaired peak prediction accuracy (UPPA) (%) (eq. 5). The continuous line is the U.S. EPA acceptance values (+20%). Values within the interval [0, $+\infty$), with a perfect peak forecast when UPPA = 0.

UPPA improvements range from 7% (AURAMS) to 50% (STEM). Again, the Kalman filtered ensemble average of the raw forecasts (E, white bar) and the ensemble mean of the Kalman filtered forecasts (EK, black bar) are the better forecasts being, along with the Kalman filter EK, the only forecasts achieving the U.S. EPA acceptance value (20%). Ensemble-averaging combined with Kalman filtering accurately forecasts peak ozone values, whereas double filtering degrades (increases) the UPPA values of the raw EK.

3.4. CSI

Larger CSI values (closer to 100%) are better. CSI gives an indication of the forecast performance for rare events, which for this study corresponds to ozone thresholds between 60 and 90 ppbv. During the ICARTT/NEAQS experiments, ozone above 60 ppbv was observed 6% of the time, whereas ozone above 90 ppbv was observed 0.1% of the time, out of a total of 421 082 valid observations. This means that the higher the threshold, the higher will be the sample uncertainty, and therefore the statistical significance gets progressively lower with higher thresholds.

The five panels on the left-hand side in Fig. 7 show the results for AURAMS, BAMS-15, BAMS-45, CHRONOS and

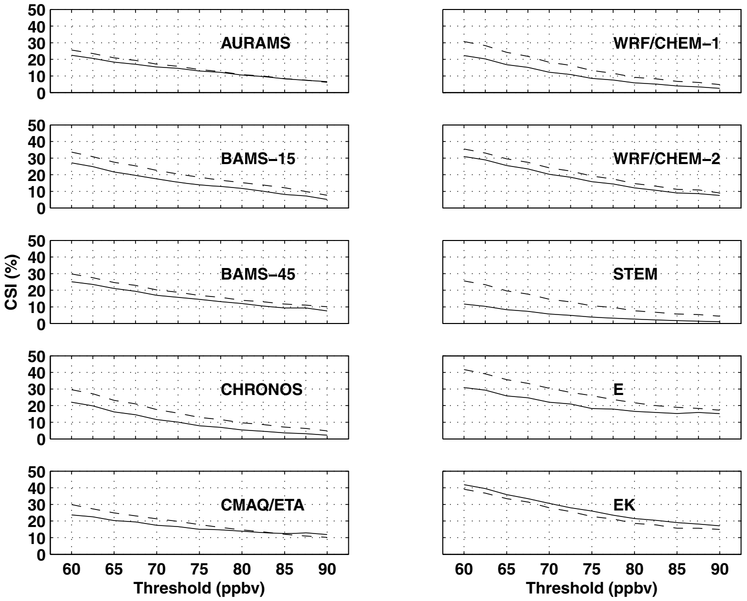

Fig. 7. Critical success index (CSI) (%) values (eq. 6) for (left-hand side: from top to the bottom panel) AURAMS, BAMS-15, BAMS-45, CHRONOS and CMAQ/ETA and for (right-hand side: from top to the bottom panel) WRF/CHEM-1, WRF/CHEM-2, STEM, the ensemble mean of the raw forecasts (E) and the Kalman filtered forecast (EK) (solid lines for the raw forecasts, dashed lines for the Kalman filtered corrected forecasts). CSI is computed for ozone above thresholds ranging from 60 to 90 ppbv, with increments of 2.5 ppbv. Values are within the interval [0, 100], with a perfect forecast when CSI = 100.

CMAQ/ETA, for the thresholds mentioned above, with increments of 2.5 ppbv. Similarly, the five panels on the right-hand side show the results for WRF/CHEM-1, WRF/CHEM-2, STEM, E and EK. The continuous lines represent the raw forecast, and the dashed lines represent the Kalman-filtered forecasts.

The filter improves the forecast performance with almost every threshold, except for CMAQ/ETA with 87.5 and 90 ppbv, and for EK for all the thresholds. The largest improvements are observed with thresholds between 60 and 75 ppbv, particularly for CHRONOS, STEM, WRF/CHEM-1 and E. Applying the filter twice (by filtering EK) does not produce any improvement. These findings are similar to what was found with the other metrics (i.e. correlation, RMSE and UPPA). Namely only one pass of the KF is needed. As already discussed, this reflects the benefits of having a long period to learn the bias behaviour, as well as the use of an optimal error-ratio value.

The raw EK and the filtered E are always the better performing forecasts with the CSI metric, underlying the usefulness of ensemble averaging combined with Kalman filtering to predict rare events regardless of the order in which these operators are applied. Among the raw deterministic forecasts, CMAQ/ETA has slightly but evident better skill than the others in predicting infrequently occurring high ozone concentration values.

4. Probabilistic forecasts

The probability of an event occurrence (e.g. ozone concentration above a certain threshold) can be computed as the ratio of the number of the ensemble members that predict the event to the total number of members (Wilks, 1995). The skill of a probabilistic forecast (PF) can be estimated by evaluating two attributes: resolution and reliability (Jolliffe and Stephenson, 2003). In the following two subsections, these important attributes are defined and measured for a PF formed by the raw forecasts (PF-R) and a PF formed by the KF-corrected forecasts (PF-KF).

4.1. Resolution

Resolution measures the ability of the forecast to sort a priori the observed events into separate groups, when the events considered have a frequency different from the climatological frequency. For an ozone PF system, two different events could be the ozone concentrations above two different thresholds (Delle Monache et al., 2006c). A PF system with good resolution should be able to separate the observed concentrations when the two different probabilities are forecasted.

Resolution can be measured with Relative Operating Characteristics (ROC), developed in the field of signal-detection theory for discrimination between two alternative outcomes (Mason, 1982). ROC compares the false alarm rate (false positives) of a set of forecasts versus the hit rate (true positives) for a given probability threshold. With an eight-member ensemble, there are nine possible probability thresholds: from 0/8 to 8/8. After the hit rate and false alarm rate are computed for each of the nine possible forecast-probability thresholds, hit rates can be plotted on the ordinate against the corresponding false-alarm rates on the abscissa to generate the ROC curve. The area under the ROC curve quantifies the ability of an ensemble to discriminate between events, which can be equated to forecast usefulness. The closer the area is to unity, the more useful is the forecast. A value of 0.5 indicates that the forecast system has no skill relative to a chance forecast from climatology. The ROC curve does not depend on the forecast bias, hence it is independent of reliability (Section 4.2). The ROC represents an intrinsic PF value.

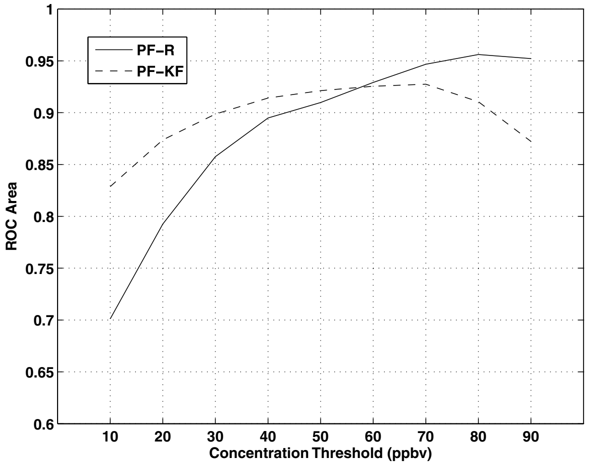

Fig. 8. Relative operating characteristics (ROC) area values for different ozone concentration thresholds (from 10 to 90 ppbv, with increments of 10 ppbv), for the probabilistic forecast formed by the raw forecasts (PF-R) (solid line) and the probabilistic forecast formed by the Kalman-filtered corrected forecasts (PF-KF) (dashed line). Values are within the interval [0, 1], with the perfect ROC-area = 1.

Figure 8 shows the ROC-area values for PF-R and PF-KF. The ROC area is computed for ozone concentration thresholds from 10 to 90 ppbv, with increments of 10 ppbv. Kalman filtering is able to considerably improve the PF predictive skill between 10 and 50 ppbv. However, from 70 to 90 ppbv it degrades the PF resolution, even though PF-KF ROC-Area values are still above 0.85 with these thresholds, indicating a forecast with high resolution. This means that the filter is not only removing the bias, but it is also modifying the predictive skill of the forecasts, by improving those below 60 ppbv, and deteriorating those above it. Wilczak et al. (2006) found similar results in ROC values using a running-mean bias-correction for ozone daily peak concentrations, using the same model predictions and observations. Resolution is not affected by removing the overall bias by definition, but since here KF is applied for each hour of the day independently, it predicts different biases for different hours and then is also able to affect the forecast resolution.

It is interesting to note that while the filter improves the deterministic and ensemble-averaged predictions of ozone peak concentration values (by looking at UPPA, Section 3.3) and for almost every ozone concentration threshold for rare events (by looking at CSI, Section 3.4) it does not improve probabilistic forecast for high (from 70 to 90 ppbv) ozone concentration thresholds (by looking at ROC). This can be explained as follows. The filter tends to increase the predicted concentration values, particularly the upper end of the distribution (not shown), bringing those values closer to the observed values. Therefore, the number of times the predicted concentration is below a given threshold tends to be reduced after the Kalman Filter (KF) correction. This results in better UPPA values after the KF correction, since UPPA is computed by looking at the 1-h maximum concentration over 1 d. CSI (for deterministic predictions) and ROC (for probabilistic predictions) are both threshold statistics, but while ROC takes into account cases where both observations and forecasts are below the given threshold, CSI does not. After the KF correction, the false alarm rate tends to decrease for thresholds from 70 to 90 ppbv, but this is offset by a bigger decrease in the hit rate, resulting in a lower ROC-area overall. The fact that after the KF correction the predicted concentrations are shifted to higher values, particularly for thresholds from 70 to 90 ppbv, does not directly affect CSI because this metric does not depend on how many prediction/observation pairs are below the prescribed concentration threshold.

4.2. *Reliability*

Reliability measures the capability of a PF to predict unbiased estimates of the observed frequency associated with different forecast probabilities. In a perfectly reliable forecast, the forecasted probability of the event should be equal to the observed frequency of the event for all the cases when that specific probability value is forecasted. Reliability alone is not sufficient to establish if a PF produces valuable forecasts or not. For instance, a system that always forecasts the climatological probability of an event is reliable, but not useful.

Reliability can be measured with a rank histogram (Hamill and Colucci, 1997; Talagrand and Vautard, 1997). First, the ensemble members are ranked for each prediction. Then, the frequency of an event occurrence in each bin of the rank histogram is computed and plotted against the bins. The number of bins equals the number of ensemble members plus one. A perfectly reliable PF shows a flat rank histogram, where the bins all have the same height. In fact, if each ensemble member represents an equally likely evolution of the ozone concentration, the observations are equally likely to fall between any two members.

Figure 9 shows the rank histogram for PF-R (black bars) and PF-KF (white bars). The PF-R forecast is positively biased, because the highest frequency is reported on the first bin and the frequency decreases with increasing bin number. This means that the observations, when ranked with the predictions at a given time and station, tend to fall more often in the lower bins, indicating over prediction.

The PF-KF rank histogram diagram is much closer to the ideal flat shape (indicated by the continuous line). This means that the filter is able to remove a good portion of the bias from the individual forecasts, and this in turn results in a much more reliable probabilistic prediction.

5. Summary and conclusions

This study presents an in-depth analysis of the KF as a post-processing predictor bias-correction method for deterministic, ensemble-averaged, and for the first time probabilistic surface ozone forecasts. The skills of raw and Kalman-filtered ozone forecasts have been evaluated against observations collected

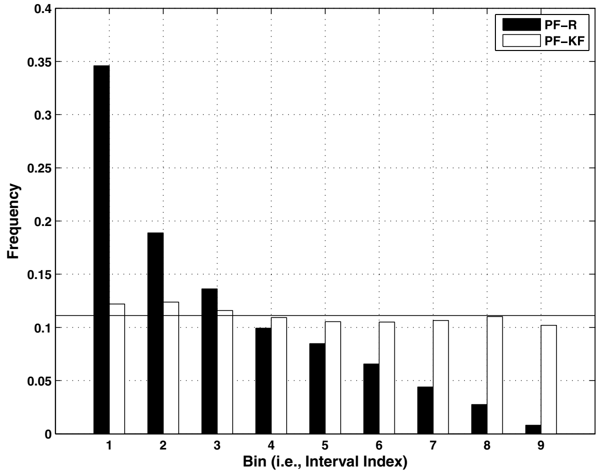

Fig. 9. Rank histogram for the probabilistic forecast formed by the raw forecasts (PF-R) (black bars) and the probabilistic forecast formed by the Kalman-filtered corrected forecasts (PF-KF) (white bars). The number of bins equals the number of ensemble members plus one. The solid horizontal line represents the perfect rank histogram shape (flat). The closer is the diagram to this horizontal line, the better is the reliability of the probabilistic forecast.

during the summer 2004 in the Northeast United States and Southeast Canada, as part of the International Consortium for Atmospheric Research on Transport and Transformation/New England Air Quality Study (ICARTT/NEAQS) (McKeen et al., 2005). The completeness of this data set, including 1-h ozone forecasts from eight different simulations for 56 d, and observations from roughly 360 stations, offered a unique opportunity to thoroughly test the filter performance. However, the summer of 2004 exhibited very few occurrences of pollution episodes because it was unseasonably cool. The statistics presented in this study are therefore specific to the summer of 2004 and might not be climatologically representative.

An optimal KF error-ratio parameter value of 0.4 has been found by evaluating the filter performance in different situations with different meteorology and different air quality (AQ) scenarios. This optimal value considerably inproved the KF performance compared to its performance with the error ratio value found in Delle Monache et al., 2006b (hereinafter referred to as DM06b), and is therefore likely to produce a better KF performance for future real-time surface ozone forecasts. However, a search of the KF optimal ratio value by analysing a data set including more typical ozone episodes may result in a different value from what has been found in this study.

Kalman filtering significantly improves the correlation (i.e. the linear dependency) between the predicted and measured ozone time series for all the forecasts [except for the Canadian Hemispheric and Regional Ozone and NO_x System (CHRONOS), and the filtered ensemble mean of the KF forecasts (EK)]. A lead/lag correlation analysis also showed that the KF-corrected ozone forecasts result in an improved accuracy in predicting the timing of concentration peak and minimum values. The forecasts having the best overall correlation are EK and the Kalman-filtered ensemble average of the raw forecasts (E). For raw deterministic forecasts the Weather Research and Forecast Model/Chemistry model version 2.03 (WRF/CHEM-2) has the best correlation, although still less than EK and E. Ensemble averaging increases the correlation with the observations for both raw and filtered forecasts.

For all the deterministic forecasts, the KF improves the ability to predict the ozone-concentration magnitude [based on the root mean square error (RMSE)]. Among the raw forecasts WRF/CHEM-2 has the lowest RMSE, while the best RMSE overall is again for the raw EK and the filtered E. The tests involving RMSE systematic ($RMSE_s$) and unsystematic ($RMSE_u$) components confirmed the results in DM06b: the filter removes a good portion of the bias while it has a minimal affects on the random errors. Vice versa, ensemble averaging tends to remove the unsystematic component of RMSE, while it leaves substantially unaltered the bias. For this reason (considering also the other statistical metrics), the combination of Kalman filtering and ensemble averaging (i.e. EK) or vice versa (i.e. the filtered E), resulted in the best forecasts in this study.

KF improves the ability to predict the daily surface ozone maximum concentration magnitude. Comparing the unpaired peak prediction accuracy (UPPA) metric results, the filtered EK has the lowest (best) value, while Baron Advanced Meteorological System Multi-scale Air Quality Simulation Platform run at 15 km (BAMS-15) has the lowest UPPA among the raw deterministic forecasts (similar to what found by Wilczak et al. (2006) using a running-mean bias-correction for the ozone maximum predictions with the ICARTT/NEAQS data set). E filtered, EK, and EK filtered are the only forecasts having UPPA values of sufficiently high accuracy that they are within the U.S. Environmental Protection Agency (EPA) acceptance value (120%, U.S. Environmental Protection Agency, 1991). This suggests the necessity of ensemble-averaging and Kalman filtering to accurately forecast the surface ozone peak magnitude.

Kalman filtering also improves the ability to predict most rare events as measured by the Critical Success Index (CSI). EK and the filtered E are always better than the other forecasts in forecasting these low-frequency events, demonstrating also in these cases the usefulness of ensemble averaging combined with Kalman filtering. The Community Multi-scale Air Quality Model (CMAQ/ETA) has the highest CSI values among the raw deterministic forecasts.

Kalman filtering is able to improve considerably the probabilistic-forecast (PF) predictive skill for ozone concentrations above thresholds from 10 to 50 ppbv. However, from 70 to 90 ppbv it degrades the PF resolution, even though the ROC-Area values are still above 0.85 with these two thresholds, indicating a forecast with high resolution. Wilczak et al. (2006) found similar results in ROC values using a running-mean bias-correction for ozone daily peak concentrations with the ICARTT/NEAQS data set.

The rank histograms show that the PF composed by raw forecasts is positively biased, whereas PF including the Kalman filtered forecasts is much closer to the ideal flat shape, meaning that the filter removes successfully most of the bias from the individual forecasts, and this in turn results in a much more reliable probabilistic prediction.

Finally, the results of this study indicate that only one application of the KF is needed to achieve the best correction (compared to earlier findings by DM06b suggesting that two applications of the filter are useful). This reflects the benefits of having a longer period to learn the bias behaviour (as with the ICARTT/NEAQS data set used here), as well as the use of an optimal error-ratio value.

The significance of KF post-processing and ensemble averaging is that they are both effective for real-time AQ forecasting. Namely, they reduce both systematic biases and random errors from coupled meteorological and Chemistry Transport Models (CTMs) to give the best estimate of future conditions, regardless of the synoptic situation and for AQ scenarios for which the underlying models were not specifically tuned.

In this work KF has been applied to improve photochemical model predictions of surface ozone. Those models are also used to produce efficient ozone controlling strategies, where different emission scenarios are considered to understand which action (e.g. anthropogenic emission reduction) would be most beneficial to reduce ozone concentrations. It is not obvious how KF could be also used for such applications and this task is left to future investigations.

6. Acknowledgments

This research is partially funded by Early Start Funding from the NOAA/NWS Office of Science and Technology and the NOAA Office of Atmospheric Research Weather and Air Quality Program and would not be possible without the participation of the AIRNow program and participating stakeholders. Credit for program support and management is given to Paula Davidson (NOAA/NWS/OST), Steve Fine (NOAA/ESRL/CSD), and Jim Meagher (NOAA/ESRL/CSD). Computational and logistic assistance from the following individuals and organizations is also gratefully appreciated: Amenda Stanley (NOAA/ESRL/GSD), Ted Smith (Baron AMS), Jessica Koury (NOAA/ESRL/PSD), Wendi Madsen (NOAA/ESRL/PSD), Ann Keane (NOAA/ESRL/PSD), Sophie Cousineau (MSC), L.-P. Crevier (MSC), Stephane Gaudreault (MSC), Mike Moran (AQRB/MSC), Paul Makar (AQRB/MSC), Balbir Pabla (AQRB/MSC), Dezso Devenyi (FSL/NOAA) and the NOAA/ESRL/GSD High Performance Computing Facility. The authors thank Véronique Bouchet for being instrumental in making the CHRONOS model output available. Thanks are also due to three anonymous reviewers for providing useful comments and suggestions. Luca Delle Monache's work was performed under the auspices of the U.S. Department of Energy by Lawrence Livermore National Laboratory under Contract DE-AC52-07NA27344.

References

Atkinson, R., Baulch, D. L., Cox, R. A., Hampson, R. F., Kerr, J. A. and co-authors. 1992. Evaluated kinetic and photochemical data for atmospheric chemistry: supplement IV. *Atmos Environ.* **26A**, 1187–1230.

Binkowski, F. S. and Shankar, U. 1995. The regional particulate model. I. Model description and preliminary results. *J. Geophys. Res.* **100**(D12), 26191–26209.

Bozic, S. M. 1994. *Digital and Kalman Filtering* 2nd Edition.Butterworth-Heinemann, New York, 160 pp.

Byun, D. W. and Schere, K. L. 2006. Description of the Models-3 Community Multiscale Air Quality (CMAQ) Model: system overview, governing equations, and science algorithms. *Appl. Mech. Rev.* **59**, 51–77.

Carmichael, G. R., Tang, Y., Kurata, G., Uno, I., Streets, D. and co-authors. 2003. Regional-scale chemical transport modeling in support of the analysis of observations obtained during the TRACE-P experiment. *J. Geophys. Res.* **108**(D21), 8823, doi:10.1029/2002JD003117.

Carter, W. 2000. Documentation of the SAPRC-99 chemical mechanism for VOC reactivity assessment. Final Report to California Air Resources Board Contract No. 92-329, University of California, Riverside.

Côté, J., Gravel, S., Méthot, A., Patoine, A., Roch, M. and co-authors. 1998a. The operational CMC-MRB Global Environmental Multiscale (GEM) model. Part I: design considerations and formulation. *Mon. Wea. Rev.* **126**, 1373–1395.

Côté, J., Desmarais, J.-G., Gravel, S., Méthot, A., Patoine, A. and co-authors. 1998b. The operational CMC/MRB Global Environmental Multiscale (GEM) model. Part II: results. *Mon. Wea. Rev.* **126**, 1397–1418.

Delle Monache, L. and Stull, R. B. 2003. An ensemble air quality forecast over western Europe during an ozone episode. *Atmos. Environ.* **37**, 3469–3474.

Delle Monache, L., Deng, X., Zhou, Y. and Stull, R. B. 2006a. Ozone ensemble forecasts: 1. A new ensemble design. *J. Geophys. Res.* **111**, D05307, doi:10.1029/2005JD006310.

Delle Monache, L., Nipen, T., Deng, X., Zhou, Y. and Stull, R. B. 2006b. Ozone ensemble forecasts: 2. A Kalman-filter predictor bias correction. *J. Geophys. Res.* **111**, D05308, doi:10.1029/2005JD006311.

Delle Monache, L., Hacker, J. P., Zhou, Y., Deng, X. and Stull, R. B. 2006c. Probabilistic aspects of meteorological and ozone regional ensemble forecasts. *J. Geophys. Res.* **111**, D24307, doi:10.1029/2005JD006917.

Gery, M. W., Whitten, G., Killus, J. and Dodge, M. 1989. A photochemical kinetics mechanism for urban and regional scale computer models. *J. Geophys. Res.* **94**, 12295–12356.

Grell, G. A., Dudhia, J. and Stauffer, D. R. 1994. A description of the fifth-generation Penn State/NCAR Mesoscale Model (MM5). NCAR Tech. Note, NCAR/TN-398+STR, 122 p.

Grell, G. A., Peckham, S. E., Schmitz, R., McKeen, S. A., Frost, G. and co-authors. 2005. Fully coupled "online" chemistry within the WRF model. *Atmos. Environ.* **39**, 6957–6975.

Hamill, T. and Colucci, S. J. 1997. Verification of Eta-RSM short-range ensemble forecasts. *Mon. Wea. Rev.* **125**, 1312–1327.

Hamill, T. M. and Snyder, C. 2000. A hybrid ensemble Kalman filter-3D variational analysis scheme. *Mon. Wea. Rev.* **128**, 2905–2919.

Homleid, M. 1995. Diurnal corrections of short-term surface temperature forecasts using Kalman filter. *Wea. Forecast.* **10**, 989–707.

Jolliffe, I. T. and Stephenson, D. B. 2003. *Forecast Verification: A Practitioner's Guide in Atmospheric Science* (eds. I. I. Jolliffe and D. B. Stephenson), Wiley and Sons, 240 p.

Lurman, F. W., Lloyd, A. C. and Atkinson, R. 1986. A chemical mechanism for use in long-range transport/acid deposition computer modeling. *J. Geophys. Res.* **91**, 10905–10936.

Mallet, V. and Sportisse, B. 2006. Ensemble-based air quality forecasts: A multimodel approach applied to ozone. *J. Geophys. Res.* **111**, D18302.

Mason, I. 1982. A model for assessment of weather forecasts. *Aust. Meteor. Mag.* **30**, 291–303.

McHenry, J. N., Ryan, W. F., Seaman, N. L., Coats, C. J., Jr. Pudykiewicz, J. and co-authors. 2004. A real-time Eulerian photochemical model forecast system. *Bull. Amer. Meteor. Soc.* **85**, 525–548.

McKeen, S. A., Wilczak, J. M., Grell, G. A., Djalalova, I., Peckham, S. and co-authors. 2005. Assessment of an ensemble of seven real-time ozone forecasts over Eastern North America during the summer of 2004. *J. Geophys. Res.* **110**, D21307, doi:10.1029/2005JD005858.

McQueen, J. and co-authors. 2004. Development and evaluation of the NOAA/EPA prototype air quality model prediction system. In: *Preprints, 20th Conference on Weather Analysis and Forecasting/16th Conference on Numerical Weather Prediction*, 12–15 January 2004, Seattle, Washington, USA.

Moran, M. D., Scholtz, M. T., Slama, C. F., Dorkalam, A., Taylor, A. and co-authors. 1997. An overview of CEPS1.0: version 1.0 of the Canadian Emissions Processing System for regional-scale air quality models. In: *Proceedings of 7th AWMA Emission Inventory Symposium*, 28–30 October 1997, Research Triangle Park, North Carolina, USA.

Pagowski, M., Grell, G. A., McKeen, S. A., Dévényi, D., Wilczak, J. M. and co-authors. 2005. A simple method to improve ensemble-based ozone forecasts. *Geophys. Res. Lett.* **32**, L07814, doi:10.1029/2004GL022305.

Pagowski, M., Grell, G. A., Devenyi, D., Peckham, S. E., McKeen, S. A. and co-authors. 2006. Application of dynamic linear regression to improve skill of ensemble-based deterministic ozone forecasts. *Atmos. Environ.* **40**, 3240–3250.

Pudykiewicz, J., Kallaur, A. and Smolarkiewicz, P. K. 1997. Semi-Lagrangian modeling of tropospheric ozone. *Tellus* **49B**, 231–258.

Roeger, C., Stull, R. B., McClung, D., Hacker, J., Deng, X. and co-authors. 2003. Verification of mesoscale numerical weather forecast in mountainous terrain for application to avalanche prediction. *Wea. Forecast.* **18**, 1140–1160.

Russell, A. and Dennis, R. 2000. NARSTO critical review of photochemical models and modeling. *Atmos. Environ.* **34**, 2283–2324.

Stockwell, W. R., Middleton, P., Chang, J. S. and Tang, X. 1995. The effect of acetyl peroxy-pperoxy radical reactions on peroxyacetyl nitrate and ozone concentrations. *Atmos. Environ.* **29**, 1591–1599.

Talagrand, O. and Vautard, R. 1997. Evaluation of probalistic prediction systems, *Proceedings ECMWF Workshop on Predictability, ECMWF,* Reading, UK, 1–25.

Thunis, P. and co-authors. 2007. Analysis of model responses to emission-reduction scenarios with in the City Delta project. *Atmos. Environ.* **41**, 208–220.

U.S. Environmental Protection Agency. 1991. Guideline for Regulatory Application Of The Urban Airshed Model. *USEPA Rep., EPA-450/4-91-013*, Research Triangle Park, North Carolina, USA.

van Loon, M., Builtjes, P. J. H. and Segers, A. J. 2000. Data assimilation applied to LOTOS: first experiences. *Environ. Model. Software* **15**, 603–609.

van Loon, M. and co-authors. 2007. Evaluation of long-term ozone simulations from seven regional air quality models and their ensemble. *Atmos. Environ.* **41**, 2083–2097.

Wilczak, J. M., McKeen, S. A., Djalalova, I. and Grell, G. 2006. Bias-corrected ensemble predictions of surface O_3. *J. Geophys. Res.* **111**, D23S28, doi:10.1029/2006JD007598.

Wilks, D. S. 1995. *Statistical Methods in the Atmospheric Sciences* (eds. R. Dmowska and J. R.Holton). Academic Press, 467 pp.

Willmott, C. J. 1981. On the validation of models. *Phys. Geogr.* **2**, 184–194.